Journal of Membrane Science 604 (2020) 118017

Contents lists available at ScienceDirect

Journal of Membrane Science

journal homepage: http://www.elsevier.com/locate/memsci

Development of graphene-PVDF composite membranes for membrane distillation

G. Grasso [a,b], F. Galiano [b], M.J. Yoo [c], R. Mancuso [a], H.B. Park [c], B. Gabriele [a,b,**], A. Figoli [b,*], E. Drioli [b,c]

[a] Laboratory of Industrial and Synthetic Organic Chemistry (LISOC), Department of Chemistry and Chemical Technologies, University of Calabria, 87036, Arcavacata di Rende, CS, Italy
[b] Institute on Membrane Technology (ITM-CNR), Via P. Bucci 17/c, 87036, Arcavacata di Rende, CS, Italy
[c] Department of Energy, Engineering, Hanyang University, Seoul, 04763, Republic of Korea

ARTICLE INFO

Keywords:
PVDF membranes
Graphene
Direct contact membrane distillation (DCMD)
Membrane preparation
Functionalized membranes

ABSTRACT

A novel PVDF-graphene composite membrane has been developed. Specifically, a commercial PVDF polymer has been suitably functionalized with the aromatic rings of styrene (PVDF-f) and characterized by spectroscopic techniques. This new material has been used as a base for the adhesion of graphene, owing to the interaction between graphene and the aromatic rings of PVDF-f. The new PVDF-f and PVDF-f-graphene (PVDF-f-G) polymers were, then, used for the preparation of porous membranes by phase inversion technique and extensively characterized by morphological, surface and chemical-physical techniques. They displayed different properties in terms of hydrophilicity, pore size and mechanical resistance. When applied in direct contact membrane distillation (DCMD), in particular, the PVDF-f-G membranes showed long-lasting salt rejection (higher than 99.9%) and higher stability in time.

1. Introduction

Water scarcity is one of the most important problems mankind is going to face in the future, and will become a more and more stringent issue due to population growth, especially in the highest density areas such as China or India [1,2]. In order to meet the increasing worldwide demand of freshwater, new strategies and efficient technologies have to be put in place aiming at preserving water natural resources and at reusing the treated wastewaters. Nowadays, membrane technology is a consolidated technique for the treatment and purification of different types of wastewaters both municipal and industrial [3–5]. Membranes, in fact, are very well appreciated over the other traditional technologies thanks to their outstanding properties in terms of selectivity, low environmental impact, flexibility and low energy requirement [2,6–8].

In the context of facing water shortage problems, desalination is becoming one of the dominant approach for the production of freshwater from seawater and brackish groundwater, considering that some countries, such as Kuwait and Qatar, already depend 100% on desalinated water [9]. The purpose of desalination is to produce pure water, which can be consumed by humans or used for domestic and industrial purposes, through the removal of salts and other minerals dissolved in it [2,10–12]. Nevertheless, thermal distillation is the oldest technique employed for desalination, it requires high energy supply which represents its main bottleneck [13].

In water desalination, in fact, the biggest challenging goals span from low energetic consumption (through the use of green energy like the solar one) to high efficiency in terms of salt rejection [14].

In this framework, membrane based processes play a pivotal role. More than 50% of the desalination plants scattered all over the world, in fact, use reverse osmosis (RO) technology for the production of freshwater [15]. Currently, RO is the leading process in water desalination [10,16], but it suffers of some important limitations such as the high operating pressures required and the relatively low efficiency due to concentration polarization phenomena [10,16,17]. Moreover, RO is limited when applied with solutions with high salinity brines (>50 g/L), since the applied hydraulic pressure can not overcome the pressure that

* Corresponding author.
** Corresponding author. Laboratory of Industrial and Synthetic Organic Chemistry (LISOC), Department of Chemistry and Chemical Technologies, University of Calabria, 87036, Arcavacata di Rende, CS, Italy.
E-mail addresses: bartolo.gabriele@unical.it (B. Gabriele), a.figoli@itm.cnr.it (A. Figoli).

https://doi.org/10.1016/j.memsci.2020.118017
Received 18 December 2019; Received in revised form 21 February 2020; Accepted 22 February 2020
Available online 20 March 2020

the membrane can tolerate (usually not higher than 80 bar) [18,19].

Alternative membrane processes, such as membrane distillation (MD), are experiencing a rapid growth in this field. MD presents some undoubted advantages such as high efficiency, low tendency to fouling and low operational temperature and pressure [10,20–25]. Moreover, MD, in comparison to other non-evaporative techniques, is able to treat high salinity brines thanks to its lower susceptibility to fouling and feed salinity [26,27].

MD is a thermally-driven process where vapor molecules migrate from the hot feed side to the cold permeate side thanks to a vapor pressure difference across the membrane. Microporous hydrophobic membranes are an essential precondition to avoid that the liquid from the feed side can pass through the membrane wetting its pores [28].

Membrane porosity, pore size and thermal insulation as well, are fundamental properties for the membranes used in MD for ensuring good performance in terms of high water vapor flux and high salt rejection. However, the lack of fully dedicated and highly optimized materials in MD represents one the obstacles to a real development of this process at industrial level.

Different approaches have been proposed so far in literature for the improvement of membranes properties and performances when applied in MD including coatings with hydrophobic perfluoropolymers [29], the use of superhydrophobic electrospun nanofibers [30], the blend with other polymers [31] and the incorporation of nanoparticles [32].

In this logic, the production of innovative composite hybrid membranes, based on the association of polymers with suitable nanomaterials (NMs), may lead to a significant improvement of the efficiency in water desalination by MD [21,32–38]. The NMs are usually dispersed in the polymer membrane matrix. Alternatively, they can be coated or grafted on the membrane surface, possibly functionalized in order to favor the NMs adhesion. Several studies, during the last years, have been focused on the possibility of using graphene for a new class of carbon based NMs [39]. Graphene consists of single-atom-thick sheets of sp^2 bonded carbon which attracted a lot of interest for electronic applications thanks to its incomparable properties [40]. The attention towards this material in membrane science stem from its potentiality to produce ultrathin membranes (with a tunable pore size acting as a molecular sieve) with superior performance in terms of permeability and selectivity [41]. Sint et al. [42], for example produced functionalized nanopores with graphene monolayers terminated with nitrogen or hydrogen and acting as ionic sieves in molecular dynamics simulation. They showed how the permeation of Li^+, K^+ and Na^+ ions was more favored for the nitrogen functionalized pores, while the permeation of Cl^- and Br^- ions was more favored for hydrogen functionalized ones. Moreover, the passage of the ions was also influenced by their size and hydration state. It was found that the selective passage of different ions through these membranes can be tailored by acting on the size and shape of nanopores, their functionalization and on the type of monolayer material.

In this work, a novel composite membrane (PVDF-f-G) was developed by grafting a suitably functionalized polyvinylidene fluoride (PVDF) membrane (PVDF-f) with graphene. The novel membrane was prepared functionalizing a commercial PVDF with aromatic rings, by treating the polymer with a strong base (KOH) to induce the formation of double bonds in the backbone by HF elimination, followed by copolymerization with styrene. Then, the adhesion between graphene and the PVDF-f membrane was performed by means of a laminating machine. The novel PVDF-f-G membrane so produced was, then, fully characterized and successfully used in direct contact membrane distillation (DCMD) operation for water desalination.

2. Materials and Methods

2.1. Chemicals

PVDF 6010 (Solef, Solvay), KOH (Daejung, 1 Kg flakes, 93% purity), azobisisobutyronitrile (AIBN) (Junsei, 1 Kg, purity ≥ 98%), styrene (Sigma Aldrich, 1 lt, purity 99.9%) and dimethylformamide (DMF) (Sigma Aldrich, purity ≥ 99.8%) have been used without further purification. For graphene synthesis, 15 μm thickness copper catalyst (Welcos, 99.9%), nitrogen (Air Korea 99.999%), argon (Air Korea 99.999%), methane (Air Korea 99.999%), hydrogen (Air Korea 99.999%) have been employed.

2.2. PVDF-f synthesis

The PVDF functionalization was realized by a two-step procedure: the first step corresponds to a basic treatment with KOH to induce the formation of double bonds in the polymeric backbone by HF elimination [43], while the second step is a radical copolymerization of the double bonds with styrene (Fig. 1) or vinylnaphthalene at different ratio (PVDF: styrene equal to 1:0.5, 1:1, 1:2 and PVDF: vinylnaphthalene equal to 1:1.15, 1:3, 1:6). In case of vinylnaphthalene the ratio considered was calculated using an equimolar concentration of styrene.

Briefly, PVDF 6010 (40 g) was suspended in a KOH solution (40 g in 719.6 g of deionized water) containing absolute EtOH (400 mg) under nitrogen atmosphere. The suspension was stirred at 60 °C for 10 min, and then a solution of PVDF (38 g) in DMF (456 mL) was slowly added in portions, followed by suitable amount of styrene (19 gr for 1:0.5 ratio, 38 gr for 1:1 ratio, 76 gr for 1:2 ratio) or equivalent amount of vinylnaphthalene and AIBN (623 mg). The resulting mixture was stirred at 70 °C for 15 h. After cooling, the polymeric material was precipitated with 2.5–3 fold excess of methanol (MeOH), then filtered, washed with DI water, and dried under vacuum at 50 °C overnight in order to obtain dry PVDF powder.

2.2.1. PVDF-f characterization – NMR

PVDF-f was characterized by NMR and FT-IR spectroscopies. ^1H and spectra were taken on a 600 MHz spectrometer (VNMRS 600 MHz) in DMF-d_7 as the solvent.

2.3. Chemical vapor deposition (CVD) - graphene synthesis

Graphene was synthetized by CVD method, using the operative conditions summarized in Fig. 2. For this purpose, high purity reagents were used: ≥ 99.999% purity argon, hydrogen and methane and 15 μm copper catalyst.

- Phase 1: 30 min, Ar flux = 500 sccm, P = 1.5 Torr, T to 750 °C
- Phase 2: 20 min, H_2 flux = 40 sccm, P = 1.5 Torr
- Phase 3: 25 min, H_2 flux = 40 sccm, P = 1.5 Torr, T = from 750 to 1020 °C
- Phase 4: 120 min, H_2 flux = 40 sccm, P = 1.5 Torr (Copper annealing phase)
- Phase 5: 30 min, H_2 flux = 120 sccm, CH_4 flux = 5 sccm P = 4.5 Torr (Graphene growth)
- Phase 6: 120–180 min, H_2 flux = 40 sccm, P = 1.5 Torr, T = from 1020 to RT

2.3.1. Graphene characterization – optical microscope

In order to evaluate graphene defects, the prepared samples were analyzed by optical microscopy. Once the procedure was completed and graphene was still on the copper foil catalyst, the sample was removed from the machine and 1 cm^2 sample was gently placed on a heating plate at 120 °C for 20 min. This led to the oxidation of copper, which assumed a darker color in the areas not directly covered by the graphene layer (as a consequence of the presence of defects), whereas the color did not change for areas beneath graphene layer (not subjected to oxidation). Eventually, in order to evaluate the presence of multilayer areas not visible unless copper removal occurs, another 1 cm^2 sample was transferred on Si wafer using wet-transfer method: preliminary this sample

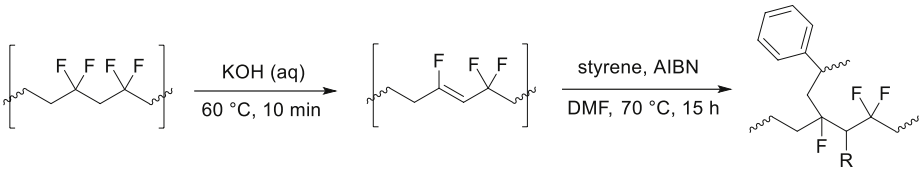

Fig. 1. Schematic representation of PVDF functionalization with styrene by basic treatment.

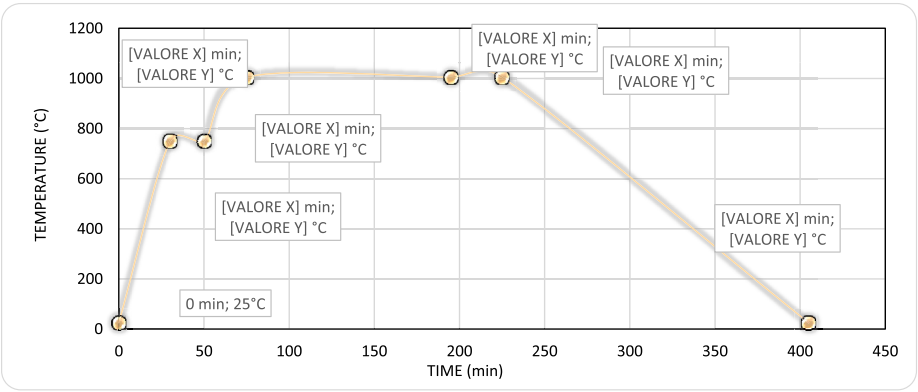

Fig. 2. Synthetic conditions used for graphene synthesis by CVD method.

was spin-coated with poly (methyl methacrylate) (PMMA) and placed on a heating plate at 120 °C to promote the adhesion between graphene and PMMA. Subsequently, the catalyst was solubilized using the procedure involving iron nitrate and iron chloride solutions below described (Section 2.4.2). Then, the PMMA-graphene sample was placed on SiO_2 wafer and on a heating plate again at 120 °C for 20 min in order to heat PMMA favoring wafer-graphene adhesion. The sample was finally plunged into a solvent able to solubilize PMMA (acetone), air dried, before being observed using optical microscope.

2.4. Membrane preparation

2.4.1. PVDF and PVDF-f flat sheet membrane preparation

Flat-sheet membranes have been produced by non-solvent induced phase separation (NIPS) technique. Dope solution was prepared using about 18% wt. polymer (pristine PVDF or PVDF-f) concentration in DMF. After stirring the solution for 12 h at 60 °C, the dope solution was cast on a glass support by using a casting machine (with a casting knife thickness of 220 μm) and immersed in a DI water bath at a temperature of about 20 °C. Once phase inversion process was completed, the membrane was first washed in an ethanol and subsequently in a hexane bath to remove the last traces of solvent. The membrane was finally dried.

2.4.2. PVDF-f-graphene thin film composite (TFC) membrane fabrication

Laminating machine (Laminatoer K-Lami customized) was used to promote adhesion between graphene and PVDF-f (*step 1*). Once the process was completed, copper was still attached to graphene and it was solubilized, using an iron chloride (III) and iron nitrate (III) solutions as etchants (*step 2*). Then, the membrane was washed several times with water and air dried overnight (*step 3*) in order to obtain the final PVDF-f membrane functionalized with graphene (PVDF-f-G). The laminating process steps are summarized in Fig. 3.

2.5. Membrane characterization

2.5.1. SEM analysis

Membrane morphology has been evaluated by scanning electron microscopy (SEM) analysis using Nova Nano SEM instrument. Samples were preventively frozen in liquid nitrogen and cut using a sharp small blade. Cross-section and top surface of the produced membranes were analyzed.

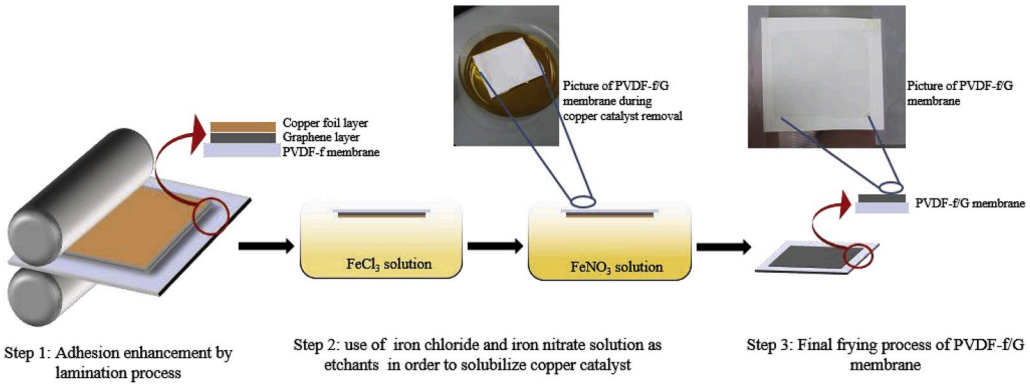

Fig. 3. PVDF-f/G membrane preparation: PVDF-f membrane adhesion with graphene carried out by laminating machine (**step 1**), copper removal by chemical etching using iron nitrate and iron chloride solutions (**step 2**), final composite membrane (PVDF-f-G) (**step 3**).

2.5.2. XPS analysis and FT-IR

X-ray photoelectron spectroscopy (XPS) analysis was performed on carbon, fluorine and oxygen atoms, in order to check the nature of bonds formed by these atoms, using a Thermo-scientific theta probe basic system. The FT-IR spectrum was registered using a Thermo-scientific Nicolet 6700 FTIR instrument.

2.5.3. Mechanical tests

In order to investigate the mechanical properties of the membranes, Young's Modulus, tensile stress at break and elongation at break have been evaluated using UTM- Shimadzu, AGS-J facility.

2.5.4. AFM analysis

Surface roughness and morphology of membranes were estimated by mean of Atomic Force Microscope (AFM) analysis, using XE-100 machine.

2.5.5. LEP and wettability

Membrane wettability is one crucial aspects in MD process since it can affect its performances, in terms of rejection and thence in terms of long-term stability. In water desalination through MD processes, hydrophobic materials such as PVDF with a high liquid entry pressure (LEP) are usually employed. LEP is the pressure that must be applied to allow the penetration of the liquid through its pores. This is a fundamental value to be considered in order to evaluate membrane efficiency, since it is comprehensive of several other factors such as hydrophobicity, geometry, pore size and distribution, surface free energy and nature of solution as well. As reported in literature, LEP was calculated by the following equation:

$$LEP = \frac{-4B\sigma\ cos\theta}{r_{max}} \quad (1)$$

where B is geometry-related factor (B = 1 for cylindrical pores), σ is solution surface-tension, Θ is contact angle and r_{max} is the largest pore diameter.

The LEP was measured through the use of a high-pressure cell (up to 5 bar) filled with water and connected to a nitrogen flask. The pressure was controlled by means of a manometer and gradually increased until the first water droplet permeating the membrane was observed.

2.5.6. DCMD experiments

Experiments were carried out using classical configuration of lab-scale DCMD facility already described in literature [44]. Briefly, the main part of the system is made by two tanks (feed and permeate) which can be heated or refrigerated selectively. One membrane-containing Teflon cell in which crossflow velocities can be regulated separately for feed and permeate side, represents the functional part of the entire machine.

DCMD tests have been performed using three different types of membranes: pristine PVDF, PVDF-f and PVDF-f-G membrane. The temperature at the permeate side was kept constant (about 20 °C) while the feed temperature was increased from 50 °C (ΔT = 30 °C) up to 70 °C (ΔT = 50 °C) with a crossflow velocity of 1 LPM and using two different solutions: DI water and salty water composed by 0.5 M NaCl aqueous solution.

Flux across the membrane is a function of water vapor pressure difference between the feed and permeate side, the membrane surface (area) and can be easily estimated using weight increase of permeate solution in the time.

The flux (J) has been calculated using the equation below:

$$J = \frac{m}{S\,t} \quad (2)$$

where m is the difference of permeate weight in the time, ρ_w is the water density, S is the membrane surface area and t is the time.

Vapor pressure difference (ΔP) was calculated according to Antoine equation [45] considering the feed and permeate temperatures:

$$P^v = \exp\left(23.38 - \frac{3841}{T - 45}\right) \quad (3)$$

where P^v is the water vapor pressure in Pascal and T is the temperature in Kelvin.

Salt rejection has been calculated using following equation:

$$R_s = (1 - C_f/C_p) * 100 \quad (4)$$

where C_f and C_p represent salt concentrations in feed and permeate side respectively.

3. Results

3.1. PVDF-f polymer preparation

As shown in Fig. 1, functionalized PVDF (PVDF-f) was prepared by a two-step procedure, involving basic treatment of commercial PVDF6010 polymer with KOH (to induce the formation of double bonds in the polymeric backbone by HF elimination), followed by radical copolymerization of the new formed double bonds with styrene (or in alternative vinylnaphthalene). Monomers bearing aromatic ring(s), like styrene or vinylnaphtalene, have been used since the adhesion between graphene layer and polymeric chain can be enhanced by π-stacking preventing any possible release of graphene.

The common methods usually employed for the preparation of membranes with graphene are represented by coating, filtration, layer-by-layer assembly and evaporation [46]. However, the approach presented in this work can be considered as one of a kind. Graphene, in fact, is not simply deposited on membrane surface (coating, filtration) but it is chemically anchored on it exploiting the stacked π- π interactions created by graphene and the PVDF-f membrane surface.

In Table 1 the different trials performed for the preparation of novel membranes (at different operating conditions and monomers used), are reported. As can be seen, the synthesis of a PVDF-f polymer which was soluble in a proper solvent and, therefore, able to produce membranes by phase inversion technique, required many efforts.

First of all, the use of vinylnaphthalene as monomer, instead of styrene, (trials 9–11) did not lead to the production of membranes at all investigated PVDF: vinylnaphtalene ratios investigated. The main issue was that, even if the synthesis of PVDF-f occurred, it exhibited so low solubility in all tested solvents (such as dimethylsulfoxide (DMSO), DMF and dimethylacetamide (DMAc)), even at high temperatures, which could not be processed for membrane preparation.

Regarding the tests where styrene was used as a monomer (trials 1–8), two main variables were considered: 1) the PVDF: styrene ratio and 2) the polymerization reaction time. Both variables, in fact, revealed to greatly affect the possibility of producing membranes since a high functionalization degree of PVDF decreased the solubility of the polymer in organic solvents. Although at all investigated PVDF: styrene ratios considered (1:0.5, 1:1 and 1:2) the polymer was successfully synthesized, not all PVDF-f polymers could be used for membrane fabrication. The PVDF-f produced at the highest reaction time considered of 24 h (trials 6–8) was not soluble in any of the solvents evaluated (DMSO, DMF and DMAc). This was probably related to the fact that, at higher polymerization times, the degree of PVDF functionalization increased leading to the formation of a series of new C–C bonds between the polymer chains and the monomer and new C–C polymer intra-chains bonds, resulting in a highly cross-linked material completely insoluble. Same reason can be ascribed to the PVDF-f prepared in trials 3 and 5, where the higher monomer concentration used (PVDF: styrene ratio 1:2), made the final polymer not suitable to be processed for membrane preparation even if the polymerization time was decreased from 24 h to 15 and 18 h, respectively. Vice versa, decreasing the monomer amount

Table 1
Synthetic conditions used for polymer synthesis.

Trial	PVDF:Monomer ratio (wt.)	Monomer type[a]	Polymerization time (h)	Polymer synthesis	Polymer solubility
1	1:0.5	Styrene	15	Yes	Yes
2	1:1	Styrene	15	Yes	Yes
3	1:2	Styrene	15	Yes	No
4	1:1	Styrene	18	Yes	Yes
5	1:2	Styrene	18	Yes	No
6	1:0.5	Styrene	24	Yes	No
7	1:1	Styrene	24	Yes	No
8	1:2	Styrene	24	Yes	No
9	1:1.15	Vinylnaphtalene	15	Yes	No
10	1:3	Vinylnaphtalene	15	Yes	No
11	1:6	Vinylnaphtalene	15	Yes	No

[a] In the case of vinylnaphtalene (trials 10–12), the amount of monomer has been calculated using an equimolar concentration with styrene.

to a ratio of 1:1 and 1:0.5, the PVDF-f produced could be completely dissolved in the selected solvent (DMF) producing a homogenous and stable dope solution.

The membranes prepared with the protocol of test 2 (PVDF/styrene ratio of 1:1, polymerization time of 15 h) were selected for the further functionalization with graphene and are the objective of all the characterization tests reported from here on out.

3.2. PVDF-f polymer characterization (^{1}H NMR)

Fig. 4 shows the ^{1}H NMR spectra of starting PVDF (pristine PDVF) a), and functionalized PVDF (PVDF-f), b).

In spectrum b, it is evident the presence of signals between 6.2 and 6.7 ppm, which are typical of aromatic protons. These signals (absent in spectrum a) are therefore ascribable to the presence of phenyl rings in the material and confirm the success of the copolymerization process between PVDF and styrene. This is further confirmed by the signals between 1.2 and 2.1 ppm in spectrum b, which are due to the –CH– and –CH_2– moieties.

3.3. Graphene characterization- optical microscope analysis

In order to estimate the presence of defects and multilayered areas, 2 × 1 cm^2 samples of graphene were analyzed after copper oxidation using optical microscope (Fig. 5a) following the procedure illustrated in Materials and Methods section 2.3.1. A second sample has been spin-coated with PMMA and placed on silicon wafer after copper solubilization occurred (Fig. 5b). For each sample, two pictures were recorded at 200x and 1000x magnification (smaller and bigger picture respectively). The analysis showed that some defects are visible only at high magnification

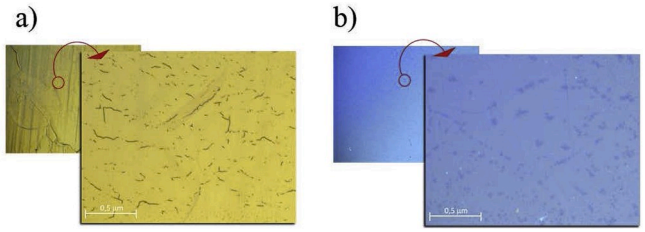

Fig. 5. Optical microscope images of graphene samples after copper oxidation a) and on silicon wafer b). (For interpretation of the references to color in this figure legend, the reader is referred to the Web version of this article.)

degree (Fig. 5a) in correspondence of areas not directly covered by graphene. In Fig. 5b, higher magnification picture shows the presence of some multi-layered areas (visible as darker blue spots) together with the presence of residual PMMA (visible as very bright light blue area in the bottom part of image).

The synthesis conditions and the type of catalyst used, led to the formation of a polycrystalline graphene: a 2D molecule that starts its growth simultaneously from different points on the catalyst surface, whose properties are ascribable to the distribution of grain boundaries typical of the CVD method [47–49].

3.4. Membrane characterization [50]

3.4.1. FT-IR and XPS

Fig. 6 shows the FT-IR spectra of pristine PVDF and PVDF-f. The presence of phenyl rings in the latter is evident from the aromatic out-of-

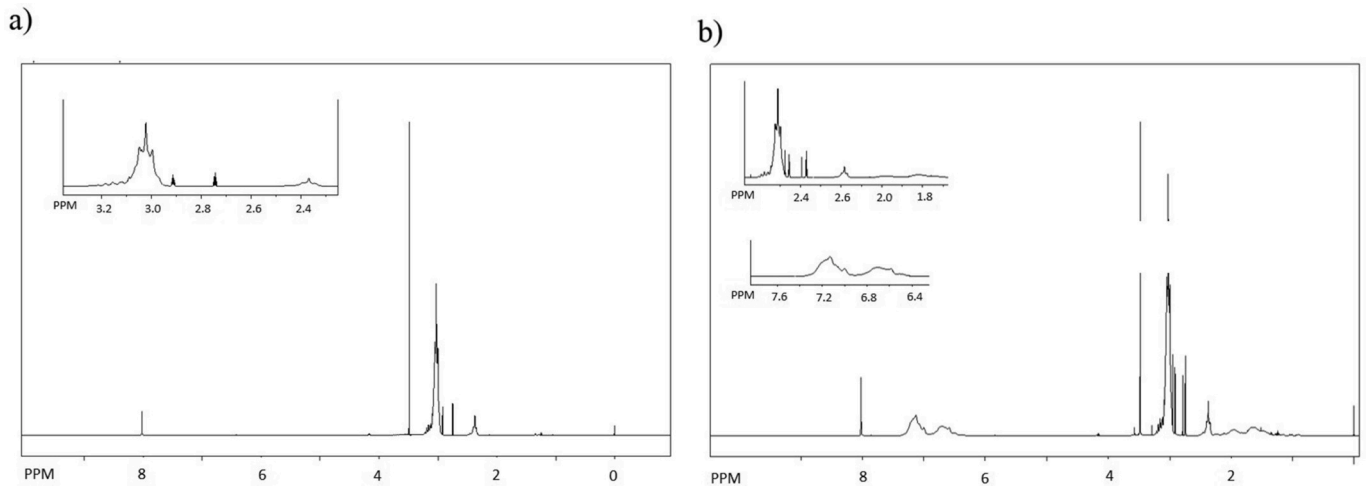

Fig. 4. ^{1}H NMR spectra for pristine PVDF (a) and PVDF-f (b).

plane C–H bending in the 700-950 cm-1 region. Spectrum differences in these areas, clearly indicate that functionalization successfully occurred since aromatic groups were successfully linked to polymer chain.

XPS analysis are shown in Fig. 7 (the general spectra of both membranes are reported in Fig. 7a). A comparison of C1s, O1s and F1s peaks for both pristine and PVDF-f are reported. In case of F1s spectra (Fig. 7c) signals are comparable, whereas O1s signal intensity (Fig. 7d) is lower in PVDF-f than pristine one. Very interesting are C1s spectra (Fig. 7b) in which PVDF CF_2 peak is visible at 290 eV, and two different peaks are shown at 284 and 285 eV, regarding styrene and CH_2 PVDF peaks respectively. In this case, the presence of three peaks in C1s spectra, indicates that functionalization occurred and aromatic groups were successfully linked to the polymer.

3.4.2. SEM and AFM

SEM and AFM representative images of the prepared membranes are shown in Fig. 8 and Fig. 9, respectively. All the membranes showed a homogeneous surface and an asymmetric structure clearly visible in cross section images (Fig. 8). Basically, the structure of the three membranes is quite similar. They are characterized by a finger-like structure located just beneath their top layer and an underlying sponge-like morphology particularly pronounced for PVDF pristine membrane which tends to fade in the PVDF-f and PVDF-f-G membranes as consequence of polymer functionalization. The presence of a finger-like structure is generally attributed to a fast liquid-liquid demixing occurring during the formation of the membrane as already observed and reported in literature [51,52]. The exchange between solvent and non-solvent, in fact, occurs rapidly on the surface of the membrane leading to an immediate precipitation of the polymer, while in the lower part of the forming membrane (bottom side) the solvent/non-solvent exchange is delayed and the finger-like architecture disappear in favor of a more sponge morphology [53]. Graphene layer was not visible on the membrane surface of PVDF-f-G membrane even at high magnification.

AFM analysis showed that the polymer functionalization was responsible of an increased membranes roughness (Fig. 9a and b). PVDF-f, in fact, presented a roughness of about 44.65 nm despite a roughness of 30.98 nm for the pristine one.

3.4.3. Contact angle (CA)

In Fig. 10, the CA for pristine PVDF (Fig. 10a), PVDF-f (Fig. 10b) and PVDF-f-G membrane (Fig. 10c) is reported. As can be seen, the functionalization of the polymer with styrene led to an increase in CA from 71° for the pristine PVDF membrane to 73° for the PVDF-f membrane. The hydrophobicity improvement is quite logic since styrene is a molecule with a hydrophobic moiety.

The functionalization with graphene (Fig. 10c), however, led to a drastic decrease of membrane CA to 61°. In the case of graphene, the precise contact angle value is still a debated question researchers are struggling with: it is well known, in fact, that CA value can heavily change on the basis of the type of graphene, the number of layers, the presence of defects, the air exposure time or even the nature of the catalyst [54–60]. The reported values of CA in literature, in fact, vary from very hydrophobic (up to 120°) to quite hydrophilic values (around 60°–70°) [56–58,61].

In an interesting study, Hong et al. [55] discussed the evolution in time of CA value for different graphene samples. For the aged graphene on Cu foil, the advancing/static/receding CA values were 84°/80°/46°, respectively. Wettability can also be affected by graphene doping, either chemical or physical. Applying a voltage to a sample of graphene lying on a SiO_2 substrate, a change of initial CA value (88°) is observed and can be ascribed to Fermi Level shifting upward or downward with respect to the Dirac Point. Both negative and positive voltage biases led to a change in terms of interaction strength between water and graphene changing therefore the wetting properties. By carrying out theoretical calculations, it was determined that the wettability (directly related to CA value) is a result of Coulomb interaction and van der Waals forces; when graphene is supported by a substrate or doped, its electron density increases and this explain the low CA value. Since the intrinsic wettability of suspended graphene is hard to evaluate, it has been found that in the CVD process, after the synthesis occurs, the cooling down process can affect the CA value: cooling under Ar atmosphere led to a higher

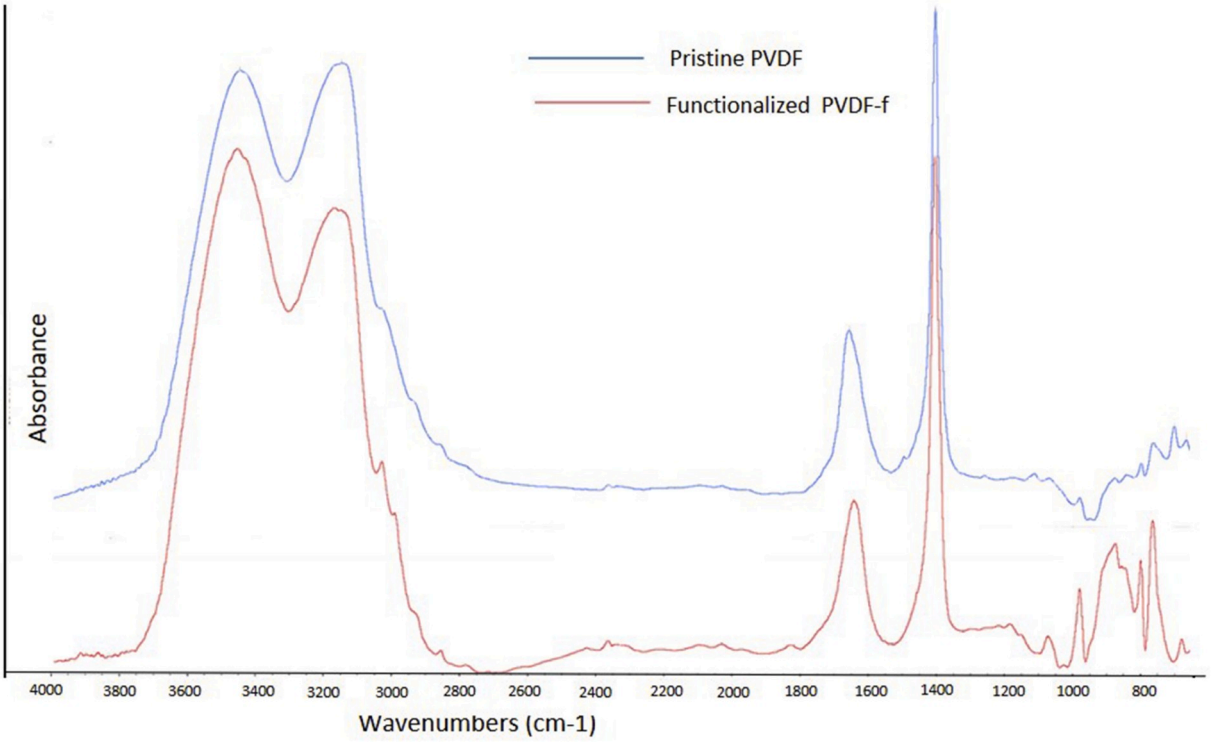

Fig. 6. Pristine PVDF- PVDF-f IR spectra comparison.

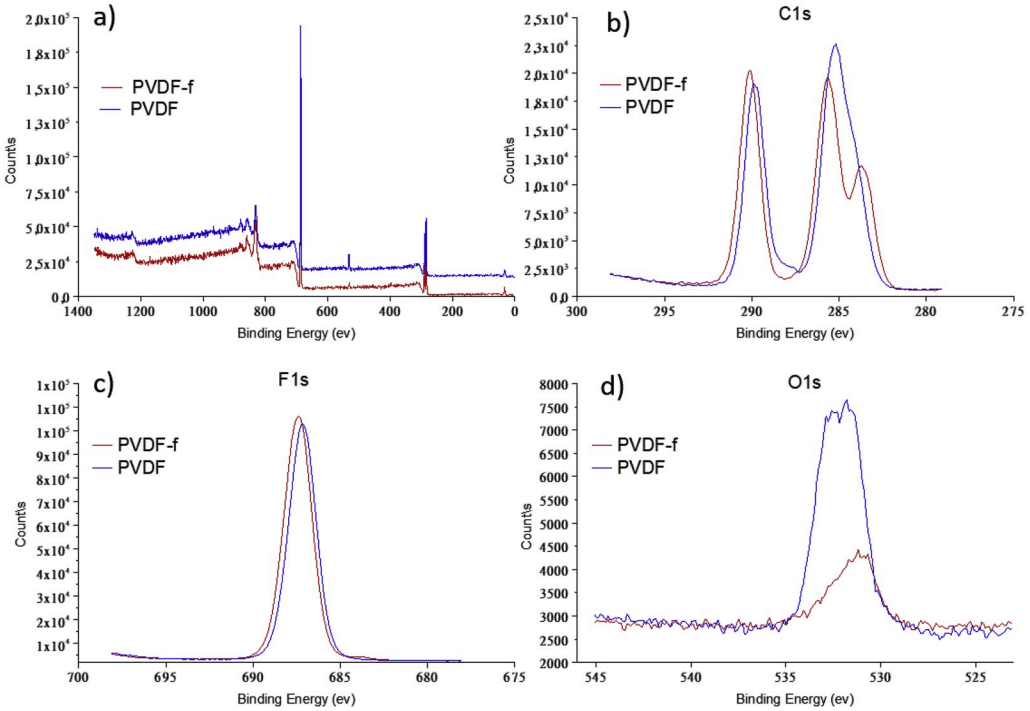

Fig. 7. General spectra (a), C1s (b), F1s (c) and O1s (d) XPS spectra for pristine and functionalized PVDF-f.

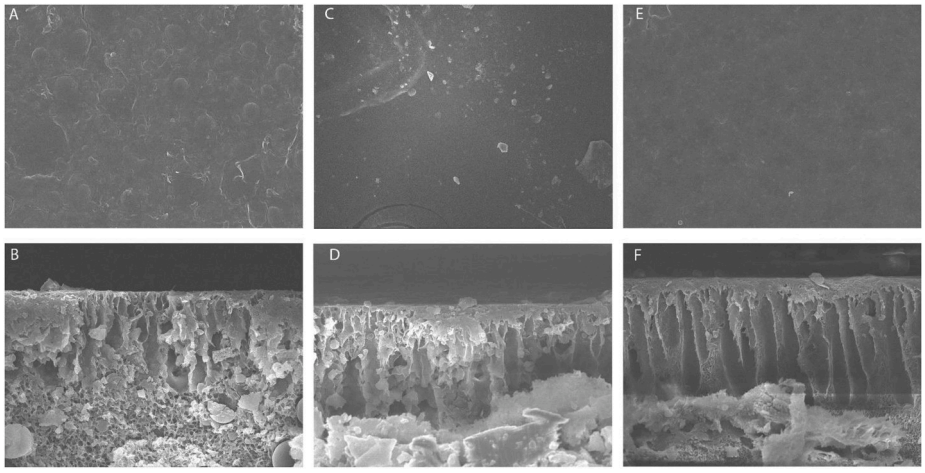

Fig. 8. SEM images of top side and cross section of pristine PVDF membrane (**a**, **b**), membrane prepared with PVDF-f (**c**, **d**), and PVDF-f-G membrane (**e**, **f**).

advancing and receding value compared to graphene cooling under H_2 atmosphere. Also, it has been reported that the CA value is affected by the number of graphene layers [62]. It has been discussed about "Wetting transparency" of graphene [63]: whenever van der Waals forces control the wetting process, and this happens for few graphene layers, the 2D material wetting behavior to the substrate is non-invasive. It results that monolayer graphene coating affects the CA value of its substrate only for 1–2%. This can find an explanation if we consider how the absorption energy of water on Cu (or any other substrate) is affected by graphene: a water molecule absorbed on Cu surface interacts with metal atoms located nearby the interaction range. With a single coated graphene layer, still these interaction forces are dominant since only the top Cu layer is covered by carbon atoms. Increasing the number of layers, the CA value is incremented because the abovementioned absorption energy decreases, as well as using a substrate like a polymer with different properties with respect to the metal substrate. In general, it is possible to accept that the conditions responsible for an increase \decrease of water absorption energy, affect the CA value.

The works cited above are important in order to understand that the contact angle for graphene depends on a series of factors often not completely and fully explained. Therefore, the low values of CA reported in this work for the PVDF-f-G membrane, does not necessarily correspond to a hydrophilic surface which could not find application in DCMD process.

3.4.4. *Mechanical tests*

Table 2 reports the mechanical tests results performed with pristine PVDF, PVDF-f and PVDF-f-G membranes expressed in terms of Young's Modulus (E-mod), tensile stress at break (Rm) and elongation at break (ε-Break). Chemical functionalization of PVDF led to a significant reduction in E-mod, Rm and ε-Break values probably due to an increased rigidity of the polymer chains as consequence of the presence of styrene aromatic rings. However, when graphene was employed, E-mod raised up as well as tensile stress at break and PVDF-f-G membrane properties

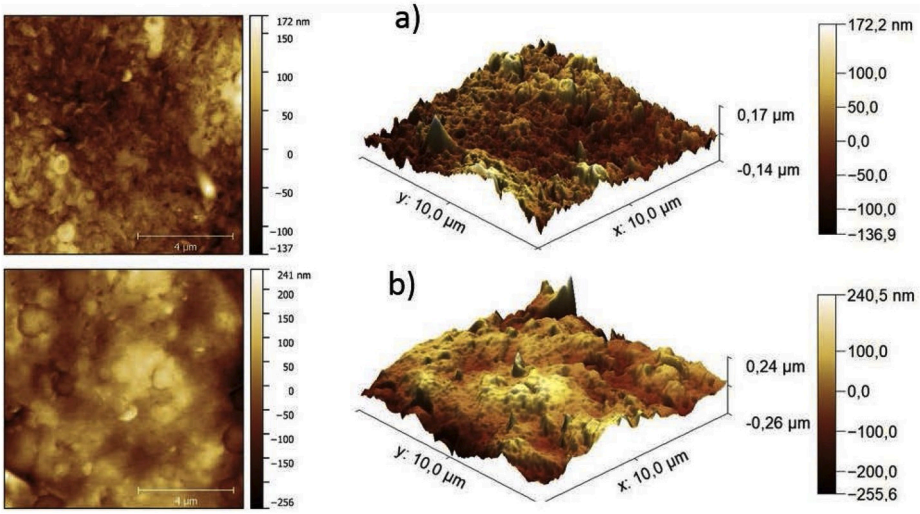

Fig. 9. AFM images of pristine PVDF (**a**) and PVDF-f (**b**) membranes.

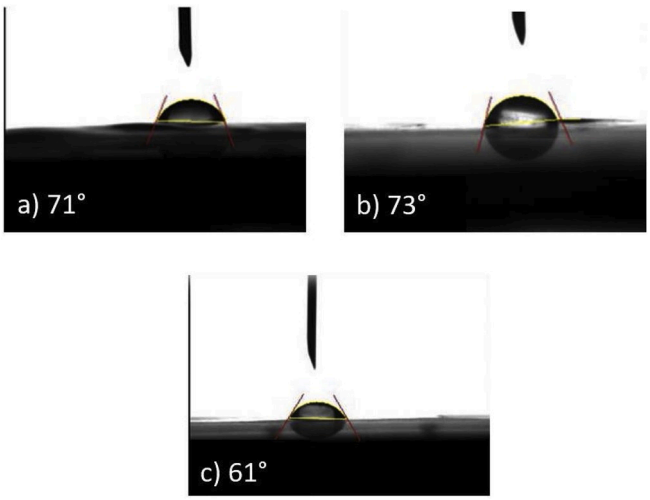

Fig. 10. Contact angle for pristine PVDF (a), PVDF-f (b) and PVDF-f-G membrane (c).

Table 2
Mechanical test results for Pristine PVDF, PVDF-f and PVDF-f-G membranes.

	E-Mod (N/mm^2)	Rm (N/mm^2)	ε- Break (%)
Pristine PVDF	208 ± 25.2	13 ± 3	141 ± 3
PVDF-f	76 ± 13	3 ± 0	61 ± 1
PVDF-f-G	143 ± 3	4 ± 0	99 ± 26

were closer to PVDF pristine membrane. It is very well known, in fact, that graphene possesses high mechanical resistance and its strong interaction with styrene can be responsible of the mechanical properties improvement.

In most of the studies reported in literature, in fact, when graphene oxide (GO) is used as a nanofiller to be incorporated into the polymer membrane matrix, an improvement of membranes mechanical properties is observed. Most of the times, this improvement is a consequence of graphene interaction with polymeric chains [64].

3.4.5. Pore size

The pore size of the produced membranes was greatly affected by the functionalization of the PVDF membrane (Table 3). PVDF-f membrane presented the highest value of mean pore size (0.13 µm) which placed it in the range of microfiltration in comparison to PVDF pristine membrane (0.03 µm) and PVDF-f-G (0.04 µm) which fell in the range of ultrafiltration.

In case of PVDF-f membrane, the steric hindrance related to the presence of the styrene molecules led to a different rearrangement of the polymer chains during the formation of the membrane resulting in a less compact structure which favored the formation of larger pores.

The addition of graphene in PVDF-f-G membranes, led, on the contrary, to a decrease in membrane pore size which showed a value of 0.04 µm.

3.5. DCMD test

DCMD tests have been performed with pristine PVDF, PVDF-f and PVDF-f-G membranes. The feed temperature was varied from 50 °C (ΔT = 30 °C) up to 70 °C (ΔT = 50 °C) with a crossflow velocity of 1 LPM and using DI water and 0.5 M NaCl aqueous solutions.

In all the tests, there is a clear difference in terms of flux between the pristine PVDF membrane and the PVDF-f and PVDF-f-G membranes. In particular, no flux was observed for the pristine PVDF membrane even increasing feed temperature. This can be due to the denser nature of the PVDF membrane which presented a measured liquid entry pressure (LEP) value of more than 5 bar. PVDF-f membrane presented the highest values of flux at all investigated temperatures (ranging from 6 to 18 L/m^2 h) due the larger pore size (0.13 µm) [29,65]. The flux, as expected, increased linearly as the temperature increased as can be also observed when the vapor differential pressure is considered (Fig. 11c) [29]. PVDF-f-G membrane presented an intermediate situation between the previous two membranes. When graphene layer was applied on membrane surface, the water flux for PVDF-f-G membrane was ranging from 1.4 to 3 L/m^2 h in case of DI (Fig. 11a) and from 0.5 to 3 L/m^2 h (Fig. 11b) in case of salty water. The lower flux exhibited by the PVDF-f-G membrane can be mainly related to two factors: the extra mass

Table 3
Pore size measurements performed on pristine PVDF, PVDF-f and PVDF-f-G membranes.

	Mean Flow Pore Pressure (bar)	Mean Pore Diameter (µm)	Blubble point pressure (bar)	Bubble Point Diameter (µm)
Pristine PVDF	15.4	0.03	1.2	0.4
PVDF-f	3.56	0.13	1.1	0.4
PVDF-f-G	10.92	0.04	1.2	0.4

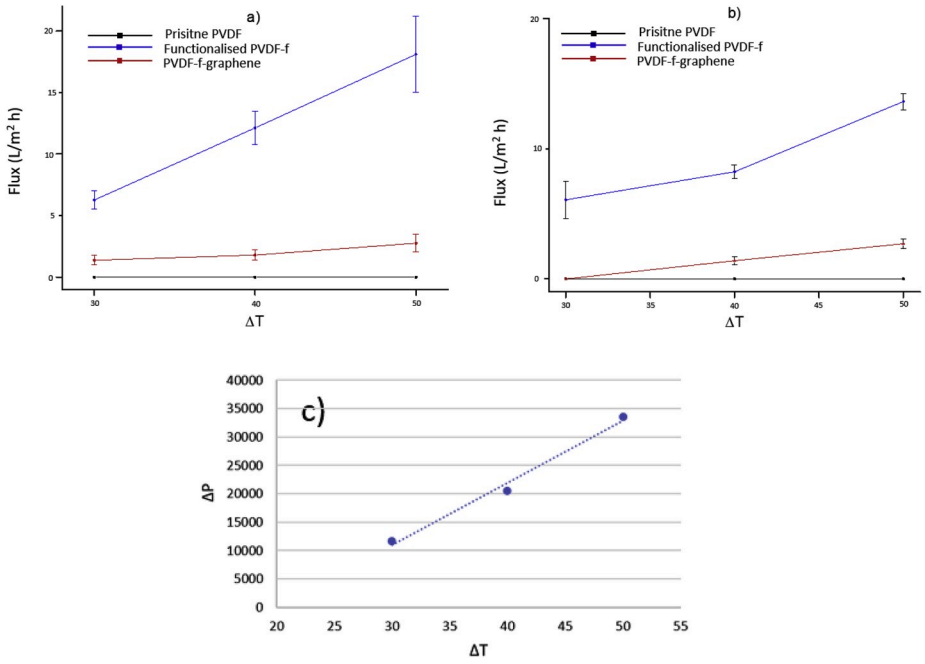

Fig. 11. MD water flux for pristine PVDF, PVDF-f and PVDF-f-G membranes with pure water a) and using 0.5 M NaCl solution b). Partial pressure difference as a function of temperature difference with pure water c).

transport resistance as consequence of graphene extra-layer on PVDF-f membrane surface; and the lower pore size showed by the membranes prepared with graphene.

Both PVDF-f and PVDF-f-G membranes presented a salt rejection higher than 99% (Fig. 12). Membranes with graphene, in particular, led to an improvement in salt rejection which was exceptionally high (close to 100%). Moreover, the PVDF-f-G membrane, even if presented lower flux in comparison to the PVDF-f one, exhibited higher stability in time keeping constant the salt rejection. The high salt rejection was also a confirmation of the good graphene deposition on the PVDF-f membrane surface which resulted in a homogenous and macroscopic defects free surface.

In literature, different works concerning membranes made with different types of PVDF and graphene for applications in MD are reported and here presented in Table 4. The membranes produced in this work (PVDF-f and PVDF-f-G) can be considered competitive if compared to most of the data obtained by other authors. In some cases, they presented better flux, better salt rejection or both (Table 4). As can be noticed, most the works reported in the table deal with PVDF membranes modified with GO or graphene quantum dots (GQDs) where graphene and graphene-like materials are usually employed as additives during dope solution preparation or immobilized on membrane surface by vacuum filtration. The approach proposed in this work can be considered unique since graphene was directly deposited and chemically

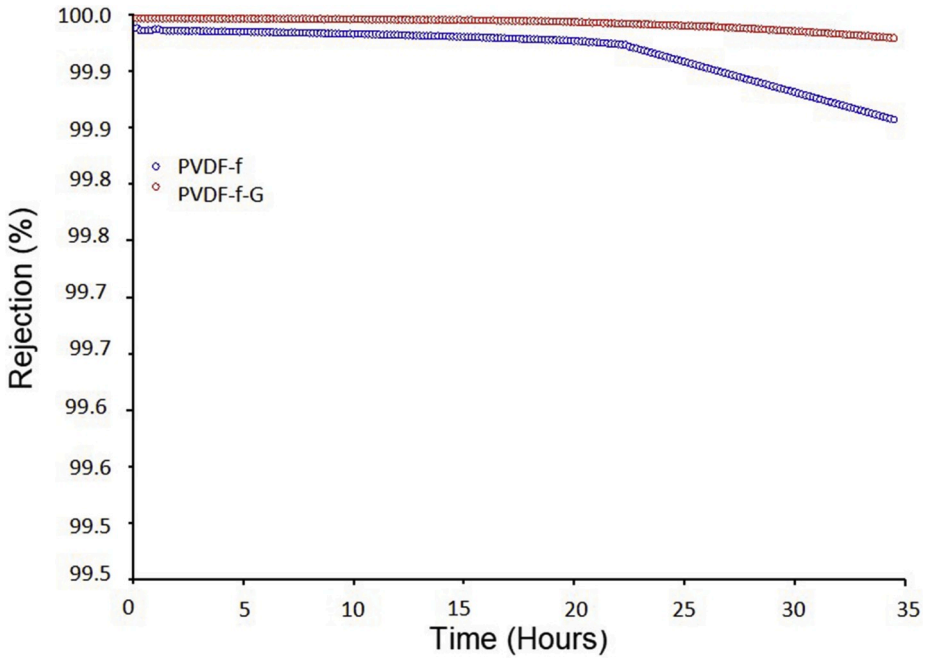

Fig. 12. Salt rejection for PVDF-f and PVDF-f-G membranes.

Table 4
Literature works comparison with PVDF membranes containing graphene, graphene-like materials or none of them.

Polymer	MD type	Salt concentration	Presence of graphene or graphene-like materials (yes/no)	Feed/Perm temperature (°C)	Flux (kg/m^2 h)	Flux/ΔP (Kg/m^2 h Pa)	Rejection	Ref.
PVDF	DCMD	0.6 M	no	50/20	1.85	$1.59{\cdot}10^{-4}$	lower than 90% using 10–15% polymer conc.	[66]
PVDF + NW fabric	DCMD	0.6 M	no	50/20	12.45	10^{-3}	lower than 90% using 10–15% polymer conc.	
PVDF	DCMD	pure water	no	50/20	10.37	$8.91{\cdot}10^{-4}$	/	[67]
PVDF + TFE	DCMD	0.3 M	no	55/20	7.2	$4.61{\cdot}10^{-4}$	close to 100%	[68]
PVDF	AGMD	0.6 M	no	60/20	from 18 to 16 after 8 h	from $8.79{\cdot}10^{-4}$ to $7.82{\cdot}10^{-4}$	PVDF from 99.5 to 94.6 after 8 h	[35]
PVDF + GQDs1 (0,05 wt%)	AGMD	0.6 M	yes	60/20	6	$2.93{\cdot}10^{-4}$	PVDF + GQD1P from 99.9% to 99.8% after 8 h	
PVDF + GQDs2 (0,1) wt%)	AGMD	0.6 M	yes	60/20	from 13 to 8 after 8 h	from $6.35{\cdot}10^{-4}$ to $3.91{\cdot}10^{-4}$	PVDF + GQD2P from 99.9% to 99.8% after 8 h	
PVDF + GQDs3 (0,25) wt%)	AGMD	0.6 M	yes	60/20	18	$8.79{\cdot}10^{-4}$	PVDF + GQD3P from 99.9% to 99.8% after 8 h	
PVDF + GQDs4 (0,5) wt%)	AGMD	0.6 M	yes	60/20	8	$3.91{\cdot}10^{-4}$	PVDF + GQD4P from 99.2% to 95.2% after 8 h	
PVDF	AGMD	0.6 M	no	85/20	3.4	$5.27{\cdot}10^{-5}$	99.9	[37]
PVDF + GO 0,1%	AGMD	0.6 M	GO (yes)	85/21	3.8	$5.91{\cdot}10^{-5}$	99.7	
PVDF + GO 0,3%	AGMD	0.6 M	GO(yes)	85/22	4.7	$7.33{\cdot}10^{-5}$	99.9	
PVDF + GO 0,5%	AGMD	0.6 M	GO(yes)	85/23	5.4	$8.45{\cdot}10^{-5}$	99.6	
PVDF + GO-APTS 0,1%	AGMD	0.6 M	GO-f (yes)	85/24	4.5	$7.06{\cdot}10^{-5}$	99.8	
PVDF + GO-APTS 0,3%	AGMD	0.6 M	GO-f (yes	85/25	6.25	$9.84{\cdot}10^{-5}$	99.9	
PVDF + GO-APTS 0,5%	AGMD	0.6 M	GO-f (yes)	85/26	5.7	$9.01{\cdot}10^{-5}$	99.7	
PVDF	DCMD	0.51 M	no	50/20	1	$8.59{\cdot}10^{-5}$	99.1	[12]
PVDF	AGMD	0.6 M	no	80/15	18.2	$3.43{\cdot}10^{-4}$	88.5	[69]
PVDF + GO-ODA M1	AGMD	0.6 M	GO-ODA (yes)	80/16	13.8	$2.60{\cdot}10^{-4}$	96.3	
PVDF + GO-ODA M2	AGMD	0.6 M	GO-ODA (yes)	80/17	16.7	$3.16{\cdot}10^{-4}$	98.3	
PVDF + GO	VMD	0.6 M	FTES-GO (yes)	50	36.4	$1.16{\cdot}10^{-3}$	99.9	[70]
PVDF + GO	AGMD	0.6 M	GO (yes)	80/20	≈7	$1.33{\cdot}10^{-4}$	99.9	[71]
PVDF-f	DCMD	0.5 M	no	70/20	≈16	$4.77{\cdot}10^{-4}$	99.9	This
PVDF-f-G	DCMD	0.5 M	yes	70/20	≈3	$8.95{\cdot}10^{-5}$	99.9	work

NW: Non-woven; AGMD: Air gap membrane distillation; ODA: Octadecylamine; GO: Graphene oxide; GO-f: Functionalized graphene oxide; GO-ODA: Octadecilamine-functionalized graphene oxide; GQDs: Graphene quantum dots; FTES-GO: 1H,1H,2H,2H-perfluorooctyltriethoxysilane (FTES) functionalized GO nanosheet; VMD: vacuum membrane distillation.

blocked on PVDF membrane surface avoiding the problems which are generally related to the use of nanoparticles (e.g. stability and release in the environment). Moreover, this procedure did not require preventively material preparation such as chemical exfoliation of graphite, treatment with strong oxidizing chemicals such as in the case of GO, purification or dispersion in solvents, since graphene was synthetized and used as coating material directly on membrane surface. This resulted in a better adhesion between graphene and membrane surface with an enhancement of the overall stability.

4. Conclusions

An innovative and simple procedure for PVDF chemical functionalization with the aim of enhancing graphene adhesion on membrane surface for fabricating new polymer-graphene composite membrane, has been conducted. Such procedure can be divided into three main steps: PVDF chemical functionalization with styrene (PVDF-f), flat sheet membrane preparation by phase inversion technique and composite membrane fabrication by graphene deposition (PVDF-f-G). The novel PVDF-f and PVDF-f-G membranes so produced were then characterized and applied in DCMD.

Practically, functionalization of PVDF with styrene introduced a certain porosity degree but also a loss of mechanical properties compared to pristine PVDF which could be recovered after adhesion with graphene. NMR and IR spectra confirmed the structure and functional groups of the newly functionalized polymer and SEM analysis showed an asymmetric architecture for all membranes mainly characterized by finger-like and spongy regions. PVDF-f membranes showed a higher degree of hydrophobicity as a consequence of styrene grafting which turned into a hydrophilicity when graphene was applied.

Membranes prepared using PVDF-f showed good water flux (16 L/m^2 h) and salt rejection higher than 99.9%. In the case of PVDF-f-G membranes, lower flux (3 L/m^2 h) was observed but accompanied to higher salt rejection in time and improved membrane performance stability.

Declaration of competing interest

The authors declare that they have no known competing financial interests or personal relationships that could have appeared to influence the work reported in this paper.

CRediT authorship contribution statement

G. Grasso: Validation, Investigation, Writing - original draft. **F. Galiano:** Investigation, Writing - original draft, Writing - review & editing. **M.J. Yoo:** Investigation, Validation. **R. Mancuso:** Investigation, Validation. **H.B. Park:** Conceptualization, Methodology, Resources, Writing - review & editing, Supervision. **B. Gabriele:** Conceptualization,

Methodology, Resources, Supervision. **A. Figoli:** Conceptualization, Methodology, Resources, Writing - review & editing, Supervision. **E. Drioli:** Conceptualization, Writing - review & editing, Supervision.

Appendix A. Supplementary data

Supplementary data to this article can be found online at https://doi.org/10.1016/j.memsci.2020.118017.

References

[1] J. Dhote, S. Ingoleb, A. Chavhan, Review on wastewater treatment technologies, Int. J. Eng. Res. Technol. 1 (2012) 1–10.

[2] M.M. Pendergast, E.M.V. Hoek, A review of water treatment membrane nanotechnologies, Energy Environ. Sci. 4 (2011) 1946, https://doi.org/10.1039/c0ee00541j.

[3] S.A. Deowan, F. Galiano, J. Hoinkis, D. Johnson, S.A. Altinkaya, B. Gabriele, N. Hilal, E. Drioli, A. Figoli, Novel low-fouling membrane bioreactor (MBR) for industrial wastewater treatment, J. Membr. Sci. 510 (2016) 524–532, https://doi.org/10.1016/j.memsci.2016.03.002.

[4] F. Galiano, I. Friha, S.A. Deowan, J. Hoinkis, Y. Xiaoyun, D. Johnson, R. Mancuso, N. Hilal, B. Gabriele, S. Sayadi, A. Figoli, Novel low-fouling membranes from lab to pilot application in textile wastewater treatment, J. Colloid Interface Sci. 515 (2018) 208–220, https://doi.org/10.1016/j.jcis.2018.01.009.

[5] J.B. Quintana, S. Weiss, T. Reemtsma, Pathways and metabolites of microbial degradation of selected acidic pharmaceutical and their occurrence in municipal wastewater treated by a membrane bioreactor, Water Res. 39 (2005) 2654–2664, https://doi.org/10.1016/j.watres.2005.04.068.

[6] A. Ali, R.A. Tufa, F. Macedonio, E. Curcio, E. Drioli, Membrane technology in renewable-energy-driven desalination, Renew. Sustain. Energy Rev. (2018), https://doi.org/10.1016/j.rser.2017.07.047.

[7] G. Daufin, J.-P. Escudier, H. Carrère, S. Bérot, L. Fillaudeau, M. Decloux, Recent and emerging applications of membrane processes in the food and dairy industry, Food Bioprod. Process. 79 (2001) 89–102, https://doi.org/10.1205/096030801750286131.

[8] F. Macedonio, E. Drioli, Pressure-driven Membrane Operations and Membrane Distillation Technology Integration for Water Purification, Desalination (2008), https://doi.org/10.1016/j.desal.2007.01.200.

[9] H. Mehdizadeh, Membrane desalination plants from an energy–exergy viewpoint, Desalination 191 (2006) 200–209, https://doi.org/10.1016/j.desal.2005.06.037.

[10] B.L. Pangarkar, M.G. Sane, M. Guddad, Reverse osmosis and membrane distillation for desalination of groundwater: a review, ISRN Mater. Sci. 2011 (2011) 1–9, https://doi.org/10.5402/2011/523124.

[11] P.K. Pandey, R. Upadhyay, Desalination of brackish water using solar energy, Int. J. Renew. Energy Resour. 6 (2016) 350–354.

[12] Y. Wu, Y. Kong, X. Lin, W. Liu, J. Xu, Surface-modified hydrophilic membranes in membrane distillation, J. Membr. Sci. 72 (1992) 189–196, https://doi.org/10.1016/0376-7388(92)80199-T.

[13] P.S. Goh, A.F. Ismail, N. Hilal, Nano-enabled membranes technology: sustainable and revolutionary solutions for membrane desalination? Desalination 380 (2016) 100–104, https://doi.org/10.1016/j.desal.2015.06.002.

[14] M.R. Qtaishat, F. Banat, Desalination by solar powered membrane distillation systems, Desalination 308 (2013) 186–197, https://doi.org/10.1016/j.desal.2012.01.021.

[15] S.S. Shenvi, A.M. Isloor, A.F. Ismail, A review on RO membrane technology: developments and challenges, Desalination 368 (2015) 10–26, https://doi.org/10.1016/j.desal.2014.12.042.

[16] X. Su, W. Li, A. Palazzolo, S. Ahmed, Concentration polarization and permeate flux variation in a vibration enhanced reverse osmosis membrane module, Desalination (2018), https://doi.org/10.1016/j.desal.2018.01.001.

[17] E.S. Jang, W. Mickols, R. Sujanani, A. Helenic, T.J. Dilenschneider, J. Kamcev, D. R. Paul, B.D. Freeman, Influence of concentration polarization and thermodynamic non-ideality on salt transport in reverse osmosis membranes, J. Membr. Sci. (2019), https://doi.org/10.1016/j.memsci.2018.11.006.

[18] T.V. Bartholomew, L. Mey, J.T. Arena, N.S. Siefert, M.S. Mauter, Osmotically assisted reverse osmosis for high salinity brine treatment, Desalination (2017), https://doi.org/10.1016/j.desal.2017.04.012.

[19] C. Fritzmann, J. Löwenberg, T. Wintgens, T. Melin, State-of-the-art of reverse osmosis desalination, Desalination (2007), https://doi.org/10.1016/j.desal.2006.12.009.

[20] S. Al-Obaidani, E. Curcio, F. Macedonio, G. Di Profio, H. Al-Hinai, E. Drioli, Potential of membrane distillation in seawater desalination: thermal efficiency, sensitivity study and cost estimation, J. Membr. Sci. (2008), https://doi.org/10.1016/j.memsci.2008.06.006.

[21] E. Curcio, E. Drioli, Membrane distillation and related operations - a review, Separ. Purif. Rev. (2005), https://doi.org/10.1081/SPM-200054951.

[22] A. Deshmukh, C. Boo, V. Karanikola, S. Lin, A.P. Straub, T. Tong, D.M. Warsinger, M. Elimelech, Membrane distillation at the water-energy nexus: limits, opportunities, and challenges, Energy Environ. Sci. (2018), https://doi.org/10.1039/c8ee00291f.

[23] A. Deshmukh, M. Elimelech, Understanding the impact of membrane properties and transport phenomena on the energetic performance of membrane distillation desalination, J. Membr. Sci. (2017), https://doi.org/10.1016/j.memsci.2017.05.017.

[24] D. González, J. Amigo, F. Suárez, Membrane distillation: perspectives for sustainable and improved desalination, Renew. Sustain. Energy Rev. (2017), https://doi.org/10.1016/j.rser.2017.05.078.

[25] I. Janajreh, R. Hashaikeh, M.N. Hussain, Evaluation of thermal efficiency of membrane distillation under conductive layer integration, in: Energy Procedia, 2017, https://doi.org/10.1016/j.egypro.2017.03.985.

[26] M. Safavi, T. Mohammadi, High-salinity water desalination using VMD, Chem. Eng. J. (2009), https://doi.org/10.1016/j.cej.2008.10.021.

[27] J. Li, Y. Guan, F. Cheng, Y. Liu, Treatment of high salinity brines by direct contact membrane distillation: effect of membrane characteristics and salinity, Chemosphere (2015), https://doi.org/10.1016/j.chemosphere.2014.12.006.

[28] A. Criscuoli, M.C. Carnevale, Desalination by vacuum membrane distillation: the role of cleaning on the permeate conductivity, Desalination 365 (2015) 213–219, https://doi.org/10.1016/j.desal.2015.03.003.

[29] A. Figoli, C. Ursino, F. Galiano, E. Di Nicolò, P. Campanelli, M.C. Carnevale, A. Criscuoli, Innovative hydrophobic coating of perfluoropolyether (PFPE) on commercial hydrophilic membranes for DCMD application, J. Membr. Sci. 522 (2017) 192–201, https://doi.org/10.1016/j.memsci.2016.08.066.

[30] Y. Liao, R. Wang, A.G. Fane, Engineering superhydrophobic surface on poly (vinylidene fluoride) nanofiber membranes for direct contact membrane distillation, J. Membr. Sci. 440 (2013) 77–87, https://doi.org/10.1016/j.memsci.2013.04.006.

[31] Z.-Q. Dong, X. Ma, Z.-L. Xu, W.-T. You, F. Li, Superhydrophobic PVDF–PTFE electrospun nanofibrous membranes for desalination by vacuum membrane distillation, Desalination 347 (2014) 175–183, https://doi.org/10.1016/j.desal.2014.05.015.

[32] A. Razmjou, E. Arifin, G. Dong, J. Mansouri, V. Chen, Superhydrophobic modification of TiO2 nanocomposite PVDF membranes for applications in membrane distillation, J. Membr. Sci. 415–416 (2012) 850–863, https://doi.org/10.1016/j.memsci.2012.06.004.

[33] D. Hou, D. Lin, C. Ding, D. Wang, J. Wang, Fabrication and characterization of electrospun superhydrophobic PVDF-HFP/SiNPs hybrid membrane for membrane distillation, Separ. Purif. Technol. (2017), https://doi.org/10.1016/j.seppur.2017.07.082.

[34] W. Intrchom, S. Roy, M. Humoud, S. Mitra, Immobilization of graphene oxide on the permeate side of a membrane distillation membrane to enhance flux, Membranes (Basel) 8 (2018) 63, https://doi.org/10.3390/membranes8030063.

[35] A. Jafari, M.R.S. Kebria, A. Rahimpour, G. Bakeri, Graphene quantum dots modified polyvinylidenefluride (PVDF) nanofibrous membranes with enhanced performance for air Gap membrane distillation, Chem. Eng. Process. - Process Intensif. (2018), https://doi.org/10.1016/j.cep.2018.03.010.

[36] C.C. Ko, A. Ali, E. Drioli, K.L. Tung, C.H. Chen, Y.R. Chen, F. Macedonio, Performance of ceramic membrane in vacuum membrane distillation and in vacuum membrane crystallization, Desalination (2018), https://doi.org/10.1016/j.desal.2018.03.011.

[37] S. Leaper, A. Abdel-Karim, B. Faki, J.M. Luque-Alled, M. Alberto, A. Vijayaraghavan, S.M. Holmes, G. Szekely, M.I. Badawy, N. Shokri, P. Gorgojo, Flux-enhanced PVDF mixed matrix membranes incorporating APTS-functionalized graphene oxide for membrane distillation, J. Membr. Sci. (2018), https://doi.org/10.1016/j.memsci.2018.03.013.

[38] F. Yang, J.E. Efome, D. Rana, T. Matsuura, C. Lan, Metal-organic frameworks supported on nanofiber for desalination by direct contact membrane distillation, ACS Appl. Mater. Interfaces (2018), https://doi.org/10.1021/acsami.8b01371.

[39] K.S. Novoselov, V.I. Fal'ko, L. Colombo, P.R. Gellert, M.G. Schwab, K. Kim, A roadmap for graphene, Nature 490 (2012) 192–200, https://doi.org/10.1038/nature11458.

[40] A.K. Geim, Graphene: status and prospects (80-.), Science 324 (2009) 1530–1534, https://doi.org/10.1126/science.1158877.

[41] T. Humplik, J. Lee, S.C. O'Hern, B.A. Fellman, M.A. Baig, S.F. Hassan, M.A. Atieh, F. Rahman, T. Laoui, R. Karnik, E.N. Wang, Nanostructured materials for water desalination, Nanotechnology 22 (2011) 292001, https://doi.org/10.1088/0957-4484/22/29/292001.

[42] K. Sint, B. Wang, P. Král, Selective ion passage through functionalized graphene nanopores, J. Am. Chem. Soc. 130 (2008) 16448–16449, https://doi.org/10.1021/ja804409f.

[43] G.J. Ross, J.F. Watts, M.P. Hill, P. Morrissey, Surface modification of poly (vinylidene fluoride) by alkaline treatment: 1. The degradation mechanism, Polymer (Guildf) (2000), https://doi.org/10.1016/S0032-3861(99)00343-2.

[44] J. Liu, X. Shen, Y. Zhao, L. Chen, Acryloylmorpholine-grafted PVDF membrane with improved protein fouling resistance, Ind. Eng. Chem. Res. (2013), https://doi.org/10.1021/ie403456n.

[45] M. Qtaishat, T. Matsuura, B. Kruczek, M. Khayet, Heat and mass transfer analysis in direct contact membrane distillation, Desalination 219 (2008) 272–292, https://doi.org/10.1016/j.desal.2007.05.019.

[46] N. Song, X. Gao, Z. Ma, X. Wang, Y. Wei, C. Gao, A review of graphene-based separation membrane: materials, characteristics, preparation and applications, Desalination 437 (2018) 59–72, https://doi.org/10.1016/j.desal.2018.02.024.

[47] Y. Zhang, L. Gomez, F.N. Ishikawa, A. Madaria, K. Ryu, C. Wang, A. Badmaev, C. Zhou, Comparison of graphene growth on single-crystalline and polycrystalline Ni by chemical vapor deposition, J. Phys. Chem. Lett. (2010), https://doi.org/10.1021/jz1011466.

[48] L. Brown, E.B. Lochocki, J. Avila, C.J. Kim, Y. Ogawa, R.W. Havener, D.K. Kim, E. J. Monkman, D.E. Shai, H.I. Wei, M.P. Levendorf, M. Asensio, K.M. Shen, J. Park,

Polycrystalline graphene with single crystalline electronic structure, Nano Lett. (2014), https://doi.org/10.1021/nl502445j.
[49] W. Wu, L.A. Jauregui, Z. Su, Z. Liu, J. Bao, Y.P. Chen, Q. Yu, Growth of single crystal graphene arrays by locally controlling nucleation on polycrystalline Cu using chemical vapor deposition, Adv. Mater. (2011), https://doi.org/10.1002/adma.201102456.
[50] F TIR, ^{1}H NMR and XPS Experiments for the PVDF-F-G Membrane (Where a Very Thin Monolayer of Graphene Was Applied) Could Not Give Additional Chemical Information on the Membrane Structure, So Only the Morphological Characterization of This Membrane by SEM Was Performed.
[51] P. Sukitpaneenit, T.-S. Chung, Molecular elucidation of morphology and mechanical properties of PVDF hollow fiber membranes from aspects of phase inversion, crystallization and rheology, J. Membr. Sci. 340 (2009) 192–205, https://doi.org/10.1016/j.memsci.2009.05.029.
[52] F. Galiano, A. Figoli, C. Conidi, F. Menichini, M. Bonesi, M.R. Loizzo, A. Cassano, R. Tundis, Functional properties of punica granatum L. juice clarified by hollow fiber membranes, Processes (2016), https://doi.org/10.3390/pr4030021.
[53] S. Simone, F. Galiano, M. Faccini, M. Boerrigter, C. Chaumette, E. Drioli, A. Figoli, Preparation and characterization of polymeric-hybrid PES/TiO2 hollow fiber membranes for potential applications in water treatment, Fibers 5 (2017) 14, https://doi.org/10.3390/fib5020014.
[54] P. Zhang, F.Y. Lv, A Review of the Recent Advances in Superhydrophobic Surfaces and the Emerging Energy-Related Applications, Energy, 2015, https://doi.org/10.1016/j.energy.2015.01.061.
[55] G. Hong, Y. Han, T.M. Schutzius, Y. Wang, Y. Pan, M. Hu, J. Jie, C.S. Sharma, U. Müller, D. Poulikakos, On the mechanism of hydrophilicity of graphene, Nano Lett. (2016), https://doi.org/10.1021/acs.nanolett.6b01594.
[56] L.A. Belyaeva, P.M.G. van Deursen, K.I. Barbetsea, G.F. Schneider, Hydrophilicity of graphene in water through transparency to polar and dispersive interactions, Adv. Mater. (2018), https://doi.org/10.1002/adma.201703274.
[57] A. Kozbial, Z. Li, C. Conaway, R. McGinley, S. Dhingra, V. Vahdat, F. Zhou, B. Durso, H. Liu, L. Li, Study on the surface energy of graphene by contact angle measurements, Langmuir (2014), https://doi.org/10.1021/la5018328.
[58] Z. Li, Y. Wang, A. Kozbial, G. Shenoy, F. Zhou, R. McGinley, P. Ireland, B. Morganstein, A. Kunkel, S.P. Surwade, L. Li, H. Liu, Effect of airborne contaminants on the wettability of supported graphene and graphite, Nat. Mater. (2013), https://doi.org/10.1038/nmat3709.
[59] F. Taherian, V. Marcon, N.F.A. Van Der Vegt, F. Leroy, What is the contact angle of water on graphene? Langmuir (2013) https://doi.org/10.1021/la304645w.
[60] K. Xu, J.R. Heath, Wetting: contact with what? Nat. Mater. (2013) https://doi.org/10.1038/nmat3763.
[61] J. Feng, Z. Guo, Wettability of graphene: from influencing factors and reversible conversions to potential applications, Nanoscale Horizons (2019), https://doi.org/10.1039/c8nh00348c.
[62] M. Munz, C.E. Giusca, R.L. Myers-Ward, D.K. Gaskill, O. Kazakova, Thickness-dependent hydrophobicity of epitaxial graphene, ACS Nano (2015), https://doi.org/10.1021/acsnano.5b03220.
[63] J. Rafiee, X. Mi, H. Gullapalli, A.V. Thomas, F. Yavari, Y. Shi, P.M. Ajayan, N. A. Koratkar, Wetting transparency of graphene, Nat. Mater. (2012), https://doi.org/10.1038/nmat3228.
[64] A. Ammar, A.M. Al-Enizi, M.A.A. AlMaadeed, A. Karim, Influence of graphene oxide on mechanical, morphological, barrier, and electrical properties of polymer membranes, Arab. J. Chem. (2016), https://doi.org/10.1016/j.arabjc.2015.07.006.
[65] M.C. García-Payo, M. Essalhi, M. Khayet, Effects of PVDF-HFP concentration on membrane distillation performance and structural morphology of hollow fiber membranes, J. Membr. Sci. (2010), https://doi.org/10.1016/j.memsci.2009.10.026.
[66] D. Hou, H. Fan, Q. Jiang, J. Wang, X. Zhang, Preparation and characterization of PVDF flat-sheet membranes for direct contact membrane distillation, Separ. Purif. Technol. (2014), https://doi.org/10.1016/j.seppur.2014.08.023.
[67] J. Phattaranawik, R. Jiraratananon, A.G. Fane, Effect of pore size distribution and air flux on mass transport in direct contact membrane distillation, J. Membr. Sci. (2003), https://doi.org/10.1016/S0376-7388(02)00603-8.
[68] C. Feng, B. Shi, G. Li, Y. Wu, Preliminary research on microporous membrane from F2.4 for membrane distillation, Separ. Purif. Technol. 39 (2004) 221–228, https://doi.org/10.1016/j.seppur.2003.12.006.
[69] J. Zahirifar, S.M.A. Moosavian, A. Hadi, P. Khadiv-Parsi, J. Karimi-Sabet, Fabrication of a novel octadecylamine functionalized graphene oxide/PVDF dual-layer flat sheet membrane for desalination via air gap membrane distillation, Desalination (2018), https://doi.org/10.1016/j.desal.2017.11.028.
[70] H. Li, W. Shi, X. Zeng, S. Huang, H. Zhang, X. Qin, Improved desalination properties of hydrophobic GO-incorporated PVDF electrospun nanofibrous composites for vacuum membrane distillation, Separ. Purif. Technol. (2020), https://doi.org/10.1016/j.seppur.2019.115889.
[71] A. Abdel-Karim, J.M. Luque-Alled, S. Leaper, M. Alberto, X. Fan, A. Vijayaraghavan, T.A. Gad-Allah, A.S. El-Kalliny, G. Szekely, S.I.A. Ahmed, S. M. Holmes, P. Gorgojo, PVDF membranes containing reduced graphene oxide: effect of degree of reduction on membrane distillation performance, Desalination (2019), https://doi.org/10.1016/j.desal.2018.11.014.